

Complexity and nonlinearity of colloid electrical transducers

Raphael Fortulan^{1a}, Noushin Raeisi Kheirabadi^a, Alessandro Chiolerio^{b,a}, Andrew Adamatzky^a

^a*Unconventional Computing Laboratory UWE Bristol UK*

^b*Bioinspired Soft Robotics Laboratory Istituto Italiano di Tecnologia Via Morego 30 16165 Genova Italy*

Abstract

This work explores the complexity and nonlinearity of seven different colloidal suspensions—Au, ferrofluid, TiO₂, ZnO, g-C₃N₄, MXene, and PEDOT:PSS—when electrically stimulated with fractal, chaotic, and random binary signals. The recorded electrical responses were analyzed using entropy, file compression, fractal dimension, and Fisher information measures to quantify complexity. The nonlinearity introduced by each colloid was evaluated by the deviation of the output from the best-fit hyperplane of the input-output mapping. The results showed that TiO₂ was the most complex colloid across all inputs, exhibiting high entropy, poor compressibility, and an unpredictable response pattern. The colloids also exhibited significant nonlinearity, making them promising candidates for reservoir computation, where the mapping of inputs into high-dimensional nonlinear states is advantageous. This study provides insight into the dynamics of colloids and their potential for unconventional computational applications that exploit their inherent complexity and nonlinearity, and it provides a rapid method for assessing the suitability of a particular material for use as a computational substrate before others.

¹Corresponding author: raphael.vicentefortulan@uwe.ac.uk

1. Introduction

Colloids, dispersed nanoparticles in a liquid, exhibit rich dynamics and physical phenomena arising from the interactions between the particles and the suspending medium. The application of external fields, such as electric or magnetic fields, can further influence the behavior of these systems, leading to the emergence of complex patterns and nonlinear responses. Harnessing these dynamics holds promise for unconventional computing paradigms, including reservoir and *in-materia* computing [1, 2, 3, 4, 5].

The notion of computing with liquid media, also known as liquid computing, dates back over 120 years to early hydraulic algebraic machines [6]. Since then, various approaches like fluid maze solvers, droplet logics, and colloid-based information processors have been explored, taking advantage of unique properties such as reconfigurability, scalability, potential low energy consumption, and inherent parallelism [7, 8]. In addition, previous works have demonstrated that colloid systems can implement synaptic learning and pattern recognition [9, 10].

In this work, we explore the complexity and nonlinearity of seven distinct colloidal suspensions—Au, ferrofluid, TiO_2 , ZnO, $g\text{-C}_3\text{N}_4$, MXene, and PEDOT:PSS—when subjected to fractal, chaotic, and random binary electrical signals. By analyzing the recorded electrical responses using various complexity measures and quantifying the degree of nonlinearity introduced by the colloids, we aim to identify the most promising colloidal systems for potential use in reservoir computing architectures. The findings from this study provide valuable insights into the rich dynamical behaviors exhibited by colloids under electrical stimulation and their suitability for unconventional computing applications.

2. Materials Fabrication

A total of seven colloids were prepared to study their complexity and nonlinearity. Each colloid preparation method is described as follows:

Au: A colloid solution of Au nanoparticles dispersed in H₂O with a particle size of 14 nm and a concentration of 0.1 mg ml⁻¹ was provided by PlasmaChem GmbH (Germany).

Ferrofluid: A ferrofluid solution containing Fe₃O₄ nanoparticles dispersed in H₂O at a concentration of 30 wt% was supplied by PlasmaChem GmbH (Germany).

TiO₂: A stable colloid of TiO₂ nanoparticles (30-50 nm), anatase phase, in H₂O 40 wt% was purchased from US Research Nanomaterials (USA).

ZnO: Sodium dodecyl sulfate (SDS, Merck) was added to deionized water to create a surfactant solution with a concentration of 0.22 wt%. The solution was then stirred continuously to homogenize. In sequence, 1 mg ZnO nanoparticles (US Research Nanomaterials, USA) were added to dimethyl sulfoxide (DMSO, US Research Nanomaterials, USA) while stirring continuously. The mixture was then stirred while 2 ml of SDS solution and 1 ml of 10 mol l⁻¹ NaOH were added. The resultant dispersion concentration was maintained constant at 0.1 mg ml⁻¹. The stirring operation was then continued for a few more hours to achieve a homogeneous dispersion of ZnO [11, 12].

g-C₃N₄: To synthesize g-C₃N₄ nanosheets, urea was first finely ground in an agate mortar and pestle. Then 25 g of the powder was placed in an alumina crucible, sealed, and heated up in a muffle furnace up to 550 °C at a rate of 25 °C min⁻¹. This temperature was maintained for 3 h to attain a yellow g-C₃N₄. The acquired g-C₃N₄ was then ground into powder using an agate mortar and pestle [13]. To achieve a suspension of g-C₃N₄ in H₂O with a concentration of 1 mg ml⁻¹, 10 mg of g-C₃N₄

was mixed with 10 ml deionized water [14].

MXene: In the first stage of MXene synthesis, a sacrificial etching process was employed. A solution of lithium fluoride (LiF, 0.8 g) in hydrochloric acid (HCl, 10 ml, 9 mol l^{-1}) was stirred for 5 min, facilitating the in situ production of a small amount of hydrofluoric acid (HF). The MAX phase powder (0.5 g Ti_3AlC_2) was then gradually added to the etching solution under continuous stirring. The sealed container was then placed on a magnetic stirrer at 35°C and 1000 rpm for 24 h. This allowed selective etching of the aluminum layers within the MAX phase by the HF [15].

Following the etching step, the resultant mixture was centrifuged (3500 rpm, 5 min) with deionized water. This procedure eliminated the etching residue and excess acid. The centrifugation cycles were repeated until the supernatant reached a neutral pH (~ 6). According to reports, the remaining supernatant is a green, stable colloidal solution of MXene flakes dispersed in water at a low concentration (1 mg ml^{-1}), indicating that delamination has been achieved [16]. The remaining, darker part, which most likely contained larger MXene nanosheets, was sonicated with 50 ml of deionized water for 1 h to encourage further delamination. The sonicated mixture was then recentrifuged to separate the water. Sediment containing MXene flakes was collected and dried in a vacuum oven at 120°C . The dried MXene powder was finally stored in a sealed container for future use [17, 18]. To prepare a suspension of MXene in dimethylformamide (DMF) at a concentration of 1 mg ml^{-1} , 10 mg of as-synthesized MXene was mixed with 10 ml DMF under stirring 1000 rpm for 24 h.

PEDOT:PSS: A high-conductivity grade solution of PEDOT:PSS, with a concentration of 3-4 wt% in H_2O , was purchased from Merck. Before conducting the studies, the suspensions were subjected to an ultrasonic bath (40 kHz, DK Sonic Ultrasonic, UK) for 30 min to guarantee uniform dispersion of the particles.

3. Experimental setup

The electrical signals were generated using an Arduino Uno R4 board (Arduino, Italy) connected via I2C to two MCP4728 12-bit quad-channel digital-to-analog converters (DACs, Microchip Technology, USA), using a 74HC595 multiplexer (Texas Instruments, USA). The output channels of the DACs were connected to amplifier/level shift circuits based on LM258AP op-amps (Texas Instruments, USA) to generate bipolar outputs of ± 5 V. Both positive and negative voltage rails were supplied by an IPS 4303 Laboratory DC Power Supply (ISO-TECH, Taiwan). The outputs were then electrically connected to the colloids using $\varnothing 10$ μm platinum/iridium-coated stainless steel probes to be used as inputs. An output probe was inserted into the colloid, and its voltage was measured using a 24-bit data logger from Pico Technology, UK.

To investigate the complexity and nonlinearity of all suspensions, three distinct signal patterns were programmed into the microcontroller: a random binary signal, a fractal curve, and a chaotic signal. The random binary signal, composed of a sequence of 1s and 0s generated randomly, aimed to probe the response of colloids to stochastic perturbations. The fractal curve, exhibiting self-similar patterns at different scales, was chosen to explore the hierarchical nature of colloidal structures. Meanwhile, the chaotic signal, characterized by its sensitive dependence on initial conditions, was intended to study the potential chaotic dynamics within the colloids.

By subjecting colloids to various stimuli, we aimed to understand their capabilities for advanced sensing and complex computation, as well as their usage in unconventional computing and reservoir computing. Each signal is described in more detail in the following sections.

3.1. Koch snowflake

Koch snowflake (or Koch curve) is one of the earliest and most famous fractal curves [19]. In this work, the curve was generated using Algorithm S1, as shown in the supporting information. The curve represented by two signals x and y was then applied to the colloid using two probes.

3.2. Lorenz system

The Lorenz system is a chaotic dynamical system and is modeled by the following set of differential equations

$$\dot{x} = \sigma(y - x), \quad (1)$$

$$\dot{y} = x(\rho - z), \quad (2)$$

$$\dot{z} = xy - \beta z, \quad (3)$$

where σ , ρ , and β are parameters. In this work, the dynamical system was implemented on the microcontroller using the 4th-order Runge-Kutta method [20] with a time step of 100 ms. The choice of parameters was $\sigma = 10$, $\rho = 28$, and $\beta = 8/3$, and the initial condition was set to $[1.2, 1.4, 1.6]^T$. The x , y , and z states were then applied to the colloid using three probes.

3.3. Random Bombardment

For the random bombardment, a random number between 0 and 255 (which corresponds to 8 bits) was selected every 500 ms, converted to its binary representation, and applied to the material using 8 probes. Bipolar logic was used, with +5 V representing the logical 1 and -5 V representing the logical 0.

4. Black-Box Complexity

We picture that the colloid is a black box that hides a function $f : V \rightarrow W$ inside. Assuming that no structural information is known about f , the only way to learn about it is by evaluating the function values of $f(x)$ at potential values $x \in V$. In addition, it is also possible to assume that the evaluation is performed by some *oracle*, from which $f(x)$ is queried, which represents the signal generator and acquisition system. The complexity of f (and by extension of the colloid) can then be inferred from a set of discrete tuples $(x_0, f(x_0)), (x_1, f(x_1)), \dots, (x_{N-1}, f(x_{N-1}))$.

For chaotic and dynamical systems—systems characterized by sensitive dependence on initial conditions and nonlinear dynamics—the definition of complexity for a time series can be split into two categories: (1) regularity and (2) predictability [21, 22]. Regularity refers to the number of repetitive patterns in the signal or the smoothness of the signal. Predictability, on the other hand, refers to the correlation present in the signal, i.e., how much information it carries about itself. In this work, several complexity measures are used to characterize the output time series data of the colloid. Fractal dimension quantifies the complexity repeated in the signal as the ratio of the log number of boxes to the log of the inverse box length, $\log(N)/\log(1/L)$ [23]. Shannon’s entropy, $H(X) = -\sum_{i=0}^{N-1} P(x_i) \log_2 P(x_i)$ [24], measures the minimum data storage requirements. Fisher information quantifies the amount of self-information carried by the system, which is anti-correlated with complexity. Compression algorithms like Gzip, bzip2, and LZMA2 assess compressibility, with more complex or random signals being less compressible. Further details on these complexity measures are available in the supporting information.

The computed entropy, gzip size, bzip size, XZ size, Fisher information, and fractal dimension of the recorded electrical signals from the colloids under fractal,

chaotic, and random stimuli are presented in Tabs. 1 to 3, respectively. The most complex colloidal suspension was chosen as the one exhibiting the highest complexity indices and was identified as the most complex. Subsequent selections proceeded accordingly.

Table 1: The calculated entropy, gzip size, bzip size, XZ size, Fisher information, and fractal dimension of the measured electrical signal of the colloids for a fractal-like signal input

Colloid	Entropy	gzip Size	bzip2 Size	XZ Size	FI	FD
Au	10.5	5.41	4.74	4.06	7.63×10^{-1}	1.02
Ferrofluid	10.5	3.53	2.99	2.71	9.00×10^{-1}	1.06
g-C ₃ N ₄	10.5	5.25	4.65	4.13	6.25×10^{-1}	1.03
MXene	10.4	5.35	4.81	4.08	4.95×10^{-1}	1.02
PEDOT:PSS	10.5	5.35	4.78	4.08	7.50×10^{-1}	1.01
TiO ₂	11.2	5.39	4.68	4.48	2.10×10^{-1}	1.05
ZnO	10.5	4.94	4.35	3.79	6.73×10^{-1}	1.03

The colloid with the highest complexity across all inputs was TiO₂. For the fractal input, Au and PEDOT:PSS secured the second and third positions, while for the chaotic input, PEDOT:PSS and Au had the second and third positions, respectively. Finally, for the random binary string input, g-C₃N₄ and Au had the second and third positions. Fig. 1 shows the recorded electrical signals of the colloids for all inputs. Visually, the highly complex behavior of the TiO₂ colloid is evident, characterized by an unpredictable pattern.

Table 2: The calculated entropy, gzip size, bzip size, XZ size, Fisher information, and fractal dimension of the measured electrical signal of the colloids for a chaotic-like signal input

Colloid	Entropy	gzip Size	bzip2 Size	XZ Size	FI	FD
Au	12.4	4.95	4.41	3.58	7.83×10^{-1}	1.02
Ferrofluid	12.4	3.44	2.88	2.62	9.47×10^{-1}	1.03
g-C ₃ N ₄	12.3	4.58	3.99	3.29	6.32×10^{-1}	1.06
MXene	12.4	4.65	4.18	3.23	7.71×10^{-1}	1.00
PEDOT:PSS	12.4	5.10	4.43	3.80	8.77×10^{-1}	1.04
TiO ₂	12.4	5.16	4.35	3.99	5.60×10^{-1}	1.07
ZnO	18.5	4.43	3.80	3.03	5.36×10^{-1}	1.02

Table 3: The calculated entropy, gzip size, bzip size, XZ size, Fisher information, and fractal dimension of the measured electrical signal of the colloids for an 8-bit random binary signal input

Colloid	Entropy	gzip Size	bzip2 Size	XZ Size	FI	FD
Au	12.6	5.92	5.05	5.32	6.16×10^{-2}	1.08
Ferrofluid	11.3	4.18	3.36	3.50	9.11×10^{-1}	1.08
g-C ₃ N ₄	20.5	5.90	5.07	5.44	1.53×10^{-3}	1.09
MXene	16.1	5.76	4.93	5.21	7.95×10^{-3}	1.11
PEDOT:PSS	12.1	5.88	5.08	5.23	1.04×10^{-1}	1.08
TiO ₂	38.0	5.87	5.05	5.34	1.23×10^{-3}	1.10
ZnO	15.9	5.68	4.86	5.11	9.75×10^{-3}	1.09

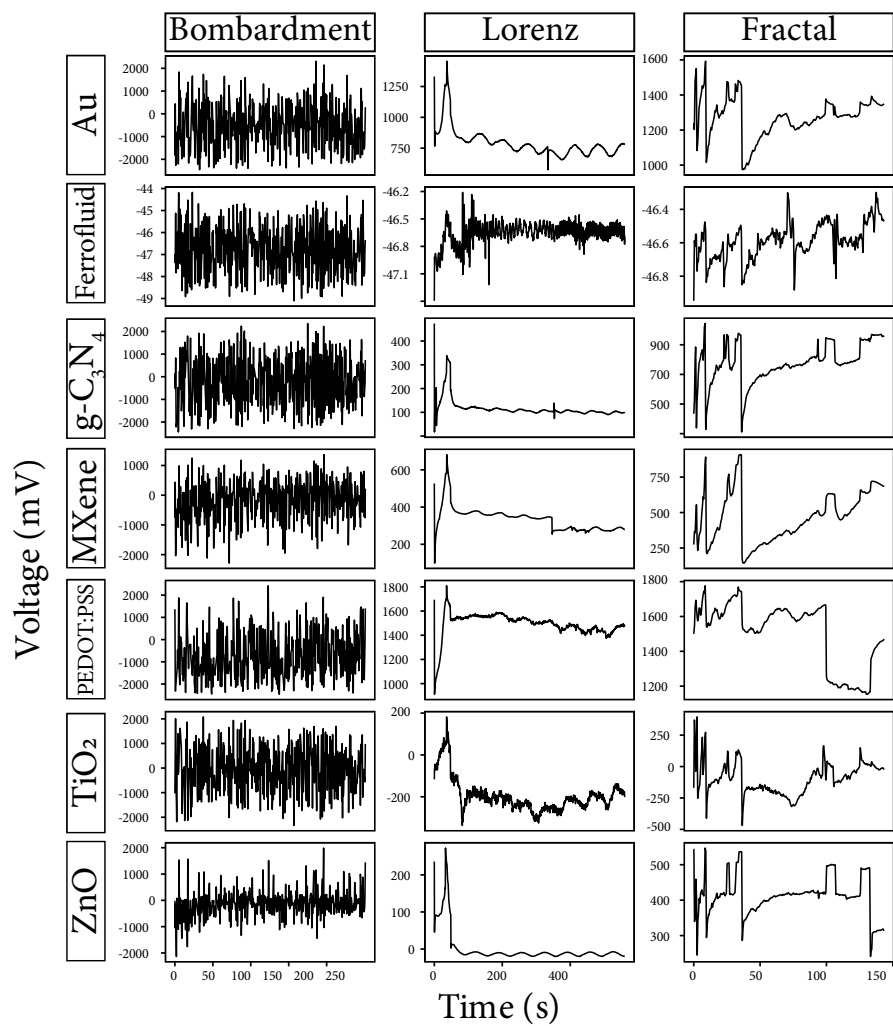


Figure 1: Measured electrical responses of the colloids for random, chaotic, and fractal signal inputs.

Fig. 2(a) shows the measured electrical response for a chaotic signal input for the TiO_2 colloid. The inset within 2(a) zooms in on a region of the curve, highlighting the complex and unpredictable nature of the colloid's behavior when subjected to electrical signals. In addition, Fig. 2(b) shows the frequency-time wavelet spectrogram of the measured electrical response for the chaotic signal applied to the TiO_2 colloid. This spectrogram provides a dynamic representation of the response of the colloid over time, highlighting the distribution of frequencies and their variations. The predominantly dark plot, with limited areas of light shading, indicates a wide dispersion of frequencies over time and a distinct lack of repetitive patterns in the data, highlighting the highly complex and dynamic nature of the response of the TiO_2 colloid and its dynamical behavior under electrical stimulation.

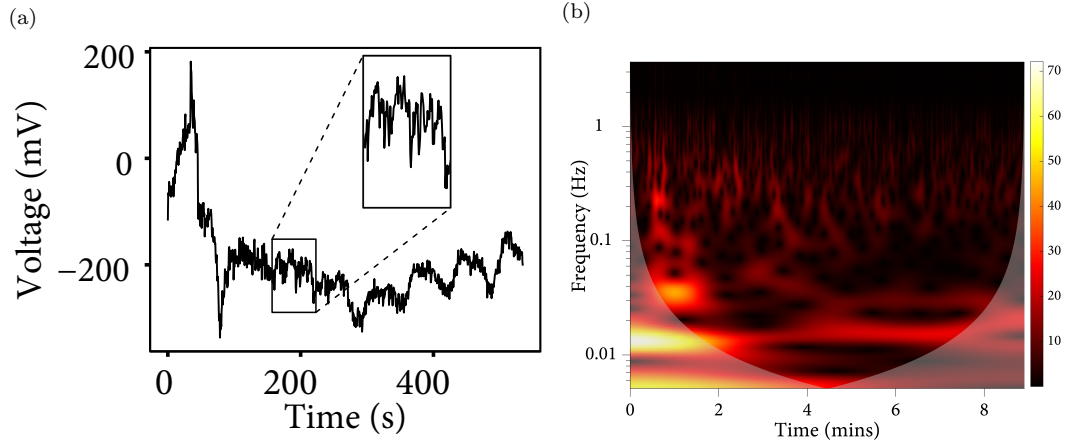


Figure 2: (a) Measured electrical response for a chaotic signal for the TiO_2 colloid. The inset shows a zoomed-in region of the curve to elucidate the complex and unpredictable pattern exhibited by the colloid when subjected to electrical signals. (b) Frequency-time wavelet spectrogram of the measured electrical response for a chaotic signal for the TiO_2 colloid. The predominantly dark plot with limited areas of light shading indicates a wide distribution of frequencies over time and a non-repetitive pattern in the data.

Tab. 4 shows the indexes calculated for the input electrical signals. As can be seen, the indexes are generally lower for the inputs than what has been observed for all colloid solutions, which indicates an increase in the complexity of the signal.

Table 4: The calculated entropy, gzip size, bzip size, XZ size, maximal Lyapunov exponent, Fisher information, and fractal dimension of the input electrical signals

Colloid	Entropy	gzip Size	bzip2 Size	XZ Size	FI	FD
Fractal	3.48	6.13×10^{-2}	7.71×10^{-2}	8.80×10^{-2}	4.25×10^{-1}	1.31
Lorenz	4.50	1.00×10^{-2}	1.43×10^{-2}	2.16×10^{-2}	5.25×10^{-1}	1.00
Random	9.99×10^{-1}	2.38×10^{-1}	2.53×10^{-1}	3.56×10^{-1}	1.28×10^{-1}	1.98

The increase in complexity was likely due to many processes occurring when an electric field is applied to the colloid. Ionizable and charged particles undergo translational movement and transient conduction due to the presence of an applied external field [25]. Dissociation of neutrals into charged species and recombination of ionized species take place in regions where the charge concentration deviates from equilibrium [26]. Charged species can also induce motion of uncharged neutral liquids, affecting charge transport and creating electrohydrodynamic conditions [27]. Particle transport can also arise from phenomena like dielectrophoresis [28], linear and nonlinear electrophoreses [29], and the Quincke rotational effect [30]. Simulating these dynamics is not an easy task [31, 32, 33, 34] thus the measurements used here provide a fast way of selecting the most complex colloids without performing time-consuming simulations.

The observed increase in entropy along with file compression sizes suggests a potential use of colloidal solutions for reservoir computing. The correlation between entropy and classifier performance is well established in the machine learning community [35] and serves as a guiding principle for model optimization and performance evaluation [36, 37]. The observed trends in entropy and file compression sizes for

the colloidal solutions for all inputs not only indicate possible good classification performance but also underscore the potential effectiveness of colloids in processing and extracting meaningful information from time series data. In addition, the data reveals a consistent trend in which the fractal dimension of the colloidal is generally lower than that of the input, suggesting the existence of memory within the colloidal solution [38]. This indicates the possibility of the usage of colloids as *in-materia* processing of time series data for high accuracy predictions [39, 40, 41, 42, 43].

5. Black-box Nonlinearity

To measure the nonlinearity introduced by the colloid solution in the applied voltage, we define a measure of the nonlinearity. Given an input vector space V , an output vector space W , and a map $M : V \rightarrow W$, the “amount” of nonlinearity of the map in a region $\alpha \subseteq V$ is defined as

$$L_\alpha^{(M)} = \left\| M(v) - P(\hat{\theta}, v) \right\|_\alpha = \sqrt{\int_\alpha \left[M(v) - P(\hat{\theta}, v) \right]^2 dv}, \quad (4)$$

where $v \in V$ and $P(\hat{\theta}, v)$ is the hyperplane that best fits the data around the region α , and it is of the following form

$$P(\hat{\theta}, v) = \sum_j \hat{\theta}^j \cdot v^j + b, \quad (5)$$

where $\hat{\theta}^j \in \hat{\theta}$ is the j -th estimated coefficient of the hyperplane, v^j is the j -th component of v , and b is an offset. In practice, we are sampling the region α around a discrete lattice, so it is safe to assume a finite number of vectors n . Then, the amount of nonlinearity can be defined as

$$L_\alpha^{(M)} = \sqrt{\sum_i \left[M(v_i) - P(\hat{\theta}, v_i) \right]^2}, \quad (6)$$

where α is no longer a continuous region in the input space but a collection of input vectors $\{v_i\}, i = 1, \dots, n$. Note that the summation in Eq. 6 may be interpreted as an approximation of the integral quantity defined in Eq. 4. Fundamentally, this nonlinearity measure shows that the output of the mapping M can be described as a linear combination of the input vectors plus a constant. Physically, this offset represents a possible potential present in the suspension when the measurement started.

Tab. 5 presents the estimated nonlinearity of the mapping of each colloidal system from the input stimulus to the measured output signal. Notably, the colloids that exhibited the highest complexity are also estimated to possess the highest amount of nonlinearity. In the context of reservoir computing, a crucial aspect of the reservoir is its capacity to perform a nonlinear mapping of the input data into a high-dimensional nonlinear state space. This nonlinear transformation of the input data enables the reservoir to capture and encode complex relationships and patterns present within the input data, allowing the subsequent linear readout layer to effectively extract and leverage these encoded features for tasks such as classification, regression, or prediction [44]. The high degree of nonlinearity of the colloids indicates their possibility for inclusion as nonlinear reservoirs in reservoir computing.

Table 5: Estimated nonlinearity of the output signal of the colloids, based on the input signals

Colloid	$L_\alpha^{(M)}$		
	Fractal	Lorenz	Bombardment
Au	1.57	2.27	13.51
Ferrofluid	0.07	0.13	0.67
g-C ₃ N ₄	2.32	2.19	15.61
MXene	3.15	4.20	9.24
PEDOT:PSS	3.54	2.56	15.43
TiO ₂	7.42	8.14	14.52
ZnO	3.27	3.88	7.79

6. Conclusions

This work investigated the complexity and nonlinearity of various colloidal suspensions subjected to different electrical signal inputs—fractal, chaotic, and random binary signals. Several complexity measures were applied to the recorded electrical output signals from the colloids, including entropy, file compression sizes, fractal dimension, and Fisher information. The most complex colloidal suspension across all input signals was found to be TiO₂, exhibiting high entropy, poor compressibility, and an unpredictable response pattern. The high complexity observed in the TiO₂ and other colloids suggests their potential usage for reservoir computing applications where transforming inputs into a high-dimensional nonlinear state space is desirable. To quantify the nonlinearity introduced by the colloids, a measure was defined based on the deviation of the output signal from the best-fit hyperplane of the input-output mapping. The results indicated that the colloids exhibiting higher complexity also

possessed a higher degree of nonlinearity in their electrical responses. Overall, this study provides insights into the complex dynamics that can emerge in colloidal suspensions under electrical stimulation. The observed high complexity and nonlinearity highlight the potential of these unconventional computing materials for applications in neuromorphic computing, time series processing, and other domains that can exploit their rich dynamical properties. Further research is warranted to better understand the underlying mechanisms driving these complex phenomena and to explore their computational capabilities in greater depth.

References

- [1] S. Stepney, Co-designing the computational model and the computing substrate, in: International Conference on Unconventional Computation and Natural Computation, Springer, 2019, pp. 5–14.
- [2] J. F. Miller, S. J. Hickinbotham, M. Amos, In materio computation using carbon nanotubes, in: Computational Matter, Springer, 2018, pp. 33–43.
- [3] J. F. Miller, The alchemy of computation: designing with the unknown, *Natural Computing* 18 (3) (2019) 515–526.
- [4] M. Lukoševičius, H. Jaeger, Reservoir computing approaches to recurrent neural network training, *Computer Science Review* 3 (3) (2009) 127–149.
- [5] N. R. Kheirabadi, A. Chiolerio, K. Szaciłowski, A. Adamatzky, Neuromorphic liquids, colloids, and gels: A review, *ChemPhysChem* 24 (1) (2023) e202200390.
- [6] A. Adamatzky, A brief history of liquid computers, *Philosophical Transactions of the Royal Society B* 374 (1774) (2019) 20180372.

- [7] R. Fortulan, N. R. Kheirabadi, P. Mougkogiannis, A. Chiolerio, A. Adamatzky, Reservoir computing with colloidal mixtures of zno and proteinoids, arXiv preprint arXiv:2312.08130 (2023).
- [8] N. Roberts, N. Raeisi Kheirabadi, M.-A. Tsompanas, A. Chiolerio, M. Crepaldi, A. Adamatzky, Logical circuits in colloids, Royal Society Open Science 11 (5) (2024) 231939. doi:10.1098/rsos.231939.
- [9] A. Chiolerio, Liquid cybernetic systems: The fourth-order cybernetics, Advanced Intelligent Systems 2 (12) (2020) 2000120.
- [10] M. Crepaldi, C. Mohan, E. Garofalo, A. Adamatzky, K. Szaciłowski, A. Chiolerio, Experimental demonstration of in-memory computing in a ferrofluid system, Advanced Materials 35 (23) (2023) 2211406.
- [11] N. R. Kheirabadi, A. Chiolerio, N. Phillips, A. Adamatzky, Learning in colloids: Synapse-like zno+ dmsO colloid, Neurocomputing 557 (2023) 126710.
- [12] N. Raeisi Kheirabadi, A. Chiolerio, A. Adamatzky, Pavlovian reflex in colloids, BioNanoScience (2024) 1–9.
- [13] N. Raeisi-Kheirabadi, A. Nezamzadeh-Ejhieh, A z-scheme g-c3n4/ag3po4 nanocomposite: its photocatalytic activity and capability for water splitting, International Journal of Hydrogen Energy 45 (58) (2020) 33381–33395.
- [14] N. R. Kheirabadi, F. Karimzadeh, M. H. Enayati, E. N. Kalali, Sustainable and photoresponse triboelectric nanogenerators based on 2d-gc3n4 and agricultural wastes, Journal of Materials Science: Materials in Electronics 34 (21) (2023) 1571.

- [15] M. Alhabeab, K. Maleski, B. Anasori, P. Lelyukh, L. Clark, S. Sin, Y. Gogotsi, Guidelines for synthesis and processing of two-dimensional titanium carbide (Ti₃C₂T_x MXene), *Chemistry of Materials* 29 (18) (2017) 7633–7644.
- [16] K. Hantanasirisakul, M. Alhabeab, A. Lipatov, K. Maleski, B. Anasori, P. Salles, C. Ieosakulrat, P. Pakawatpanurut, A. Sinitskii, S. J. May, et al., Effects of synthesis and processing on optoelectronic properties of titanium carbonitride MXene, *Chemistry of Materials* 31 (8) (2019) 2941–2951.
- [17] Y. Dong, S. S. K. Mallineni, K. Maleski, H. Behlow, V. N. Mochalin, A. M. Rao, Y. Gogotsi, R. Podila, Metallic MXenes: A new family of materials for flexible triboelectric nanogenerators, *Nano Energy* 44 (2018) 103–110.
- [18] C. Jiang, C. Wu, X. Li, Y. Yao, L. Lan, F. Zhao, Z. Ye, Y. Ying, J. Ping, All-electrospun flexible triboelectric nanogenerator based on metallic MXene nanosheets, *Nano Energy* 59 (2019) 268–276.
- [19] Š. Ungar, The Koch Curve: A Geometric Proof, *The American Mathematical Monthly* 114 (1) (2007) 61–66. [arXiv:27642119](https://arxiv.org/abs/27642119).
- [20] R. Burden, J. Faires, *Numerical Analysis*, Cengage Learning, 2010.
- [21] E. M. Bollt, Regularized forecasting of chaotic dynamical systems, *Chaos, Solitons & Fractals* 94 (2017) 8–15. [doi:10.1016/j.chaos.2016.10.007](https://doi.org/10.1016/j.chaos.2016.10.007).
- [22] M. Sobottka, L. P. L. de Oliveira, Periodicity and Predictability in Chaotic Systems, *The American Mathematical Monthly* 113 (5) (2006) 415–424. [arXiv:27641949](https://arxiv.org/abs/27641949), [doi:10.2307/27641949](https://doi.org/10.2307/27641949).

- [23] J. Wu, X. Jin, S. Mi, J. Tang, An effective method to compute the box-counting dimension based on the mathematical definition and intervals, *Results in Engineering* 6 (2020) 100106. doi:10.1016/j.rineng.2020.100106.
- [24] C. E. Shannon, A mathematical theory of communication, *The Bell System Technical Journal* 27 (3) (1948) 379–423. doi:10.1002/j.1538-7305.1948.tb01338.x.
- [25] M. Z. Bazant, T. M. Squires, Induced-charge electrokinetic phenomena, *Current Opinion in Colloid & Interface Science* 15 (3) (2010) 203–213.
- [26] V. Novotny, Contributions of particles to electrical conductivity of colloids, *Colloids and Surfaces* 21 (1986) 219–233. doi:10.1016/0166-6622(86)80093-2.
- [27] P. Atten, Electrohydrodynamic stability of dielectric liquids during transient regime of space-charge-limited injection, *The Physics of Fluids* 17 (10) (1974) 1822–1827. doi:10.1063/1.1694623.
- [28] O. P. Pishnyak, S. V. Shiyanovskii, O. D. Lavrentovich, Aggregation of colloidal particles in a non-equilibrium backflow induced by electrically-driven reorientation of the nematic liquid crystal, *Journal of Molecular Liquids* 164 (1) (2011) 132–142. doi:10.1016/j.molliq.2011.09.005.
- [29] A. S. Khair, Nonlinear electrophoresis of colloidal particles, *Current Opinion in Colloid & Interface Science* 59 (2022) 101587. doi:10.1016/j.cocis.2022.101587.
- [30] G. E. Pradillo, H. Karani, P. M. Vlahovska, Quincke rotor dynamics in confinement: Rolling and hovering, *Soft Matter* 15 (32) (2019) 6564–6570. doi:10.1039/C9SM01163C.

- [31] J. Zhou, R. Schmitz, B. Dünweg, F. Schmid, Dynamic and dielectric response of charged colloids in electrolyte solutions to external electric fields, *The Journal of Chemical Physics* 139 (2) (2013) 024901. doi:10.1063/1.4812692.
- [32] J. Zhou, F. Schmid, Dielectric response of nanoscopic spherical colloids in alternating electric fields: A dissipative particle dynamics simulation, *Journal of Physics: Condensed Matter* 24 (46) (2012) 464112. doi:10.1088/0953-8984/24/46/464112.
- [33] K. S. Krishnamurthy, D. S. Shankar Rao, M. B. Kanakala, C. V. Yelamaggad, Electric response of topological dipoles in nematic colloids with twist-bend nematic droplets as the dispersed phase, *Physical Review E* 103 (4) (2021) 042701. doi:10.1103/PhysRevE.103.042701.
- [34] S. Dutta, J. Chakrabarti, Transient dynamical responses of a charged binary colloid in an electric field, *Soft Matter* 14 (22) (2018) 4477–4482. doi:10.1039/C7SM02552A.
- [35] F. J. Baldán, J. M. Benítez, Complexity measures and features for times series classification, *Expert Systems with Applications* 213 (2023) 119227. doi:10.1016/j.eswa.2022.119227.
- [36] Y. Karaca, Y.-D. Zhang, K. Muhammad, Characterizing Complexity and Self-Similarity Based on Fractal and Entropy Analyses for Stock Market Forecast Modelling, *Expert Systems with Applications* 144 (2020) 113098. doi:10.1016/j.eswa.2019.113098.
- [37] Y. Karaca, D. Baleanu, A novel R/S fractal analysis and wavelet entropy char-

- acterization approach for robust forecasting based on self-similar time series modeling, *Fractals* 28 (08) (2020) 2040032. doi:10.1142/S0218348X20400320.
- [38] B. Qian, K. Rasheed, Hurst exponent and financial market predictability, in: IASTED conference on Financial Engineering and Applications, Proceedings of the IASTED International Conference Cambridge, MA, 2004, pp. 203–209.
- [39] E. Diaconescu, The use of NARX Neural Networks to predict Chaotic Time Series, *WSEAS Transactions on Computer Research* 3 (3) (2008).
- [40] I. Ghosh, M. K. Sanyal, R. K. Jana, Fractal Inspection and Machine Learning-Based Predictive Modelling Framework for Financial Markets, *Arabian Journal for Science and Engineering* 43 (8) (2018) 4273–4287. doi:10.1007/s13369-017-2922-3.
- [41] B. Qian, K. Rasheed, Stock market prediction with multiple classifiers, *Applied Intelligence* 26 (1) (2007) 25–33. doi:10.1007/s10489-006-0001-7.
- [42] S. Raubitzek, T. Neubauer, A fractal interpolation approach to improve neural network predictions for difficult time series data, *Expert Systems with Applications* 169 (2021) 114474. doi:10.1016/j.eswa.2020.114474.
- [43] S. Raubitzek, T. Neubauer, Taming the Chaos in Neural Network Time Series Predictions, *Entropy* 23 (11) (2021) 1424. doi:10.3390/e23111424.
- [44] G. Tanaka, T. Yamane, J. B. Héroux, R. Nakane, N. Kanazawa, S. Takeda, H. Numata, D. Nakano, A. Hirose, Recent advances in physical reservoir computing: A review, *Neural Networks* 115 (2019) 100–123. doi:10.1016/j.neunet.2019.03.005.